PAPER

Flexible supercapacitors based on low-cost tape casting of high dense carbon nanofibers

Materials Research Express

PAPER

RECEIVED
25 November 2016

REVISED
9 January 2017

ACCEPTED FOR PUBLICATION
24 January 2017

PUBLISHED
13 February 2017

Flexible supercapacitors based on low-cost tape casting of high dense carbon nanofibers

Allan Daraghmeh[1], Shahzad Hussain[1], Llorenç Servera[3], Elena Xuriguera[1], Mireia Blanes[2], Francisco Ramos[2], Albert Cornet[1] and Albert Cirera[1]

[1] Departament of Engineering: Electronics, IN2UB, Universitat de Barcelona, Martí i Franquès 1, 08028 Barcelona, Spain
[2] Francisco Albero S.A., L'Hospitalet de Llobregat, Rafael Barradas 19, 08908, Spain
[3] EUSS, Passeig Sant Joan Bosco, 74, 08217 Barcelona Spain

E-mail: allan.daraghmeh@ub.edu **(A Daraghmeha)**

Keywords: carbon nanofibers, flexible hybrid supercapacitors, manganese dioxide, Raman analysis, aqueous electrolyte, electrochemical properties

Abstract

This experimental study, reports the use of flexible tape casting of dense carbon nanofiber (CNFs) alone and in hybrid structure with MnO_2 for supercapacitor applications. Different electrolyte concentrations of potassium hydroxide (KOH) were tested and it was founded that mild concentrated electrolyte, like 9 M KOH, provides higher specific capacitance 38 F g^{-1} at a scan rate of 5 mV s^{-1}. Electrochemical impedance spectroscopy (EIS) measurements explain that the solution resistance and the charge transfer resistance is higher for 3 M KOH concentrations and lower for 6 M KOH concentrations. Afterwards a novel, fast and simple method is adopted to achieve a hybrid nanostructure of CNFs/MnO_2 with various $KMnO_4$ ratios. The hybrid supercapacitor, having loaded a mass of 0.0003 g MnO_2 as a thin film, delivers a highest specific capacitance of 812 F g^{-1} at a scan rate 5 mV s^{-1}. Charge/discharge cycling stability at current density of 7.9 A g^{-1} demonstrates larger specific capacitance 303 F g^{-1} and stability. Furthermore, the hybrid supercapacitor can deliver specific energy (72.4 Wh kg^{-1}) at specific power (3.44 kW kg^{-1}). Specific surface area increase from 68 m^2 g^{-1} for CNFs to 240 m^2 g^{-1} for CNFs/MnO_2.

1. Introduction

The wearable devices that intercommunicate with each other are growing rapidly [1]. One of the major challenges is to relate the energy storage system with mechanical flexibility and easy to integrate into wearable devices. Various studies are trying to develop flexible structures to obtain a fast recharge, durable and safe supercapacitors. Different carbon structures have been used to manufacture the electrode for supercapacitors, such as activated carbon [2], carbon nanotube (CNT) [3–5], carbon nanofibers (CNF) [6], graphene [7] and carbon aerogel [8, 9]. Batteries and supercapacitors perform their operations on the ion-exchange and the reduction–oxidation reactions at the surface of the electrode. A key factor to capture a large number of ions in the interface between the electrode and the electrolyte is the specific surface of the electrode. The specific surface is directly proportional to the capacity to accumulate electric charges. Nevertheless, the specific surface must be accessible for the ions, to develop porous surfaces, where ion kinetics is enhanced by the porosity [10]. The carbon material which has good combination of high microporosity, well maintained mesoporous structure and active nitrogen functional groups can show better properties for supercapacitor applications [8, 9]. The combination of porosity and porous size has to be adapted to the ions size, which will be carried by the electrolytic solution.

According to the mechanism used to store the electric charge, the electrochemical capacitors can be classified into two types: (1) electric double layer capacitors (EDLCs) works based on an electrostatic attraction between the ions and the surface of the electrode. (2) Pseudo-capacitors exhibit charge transfer reactions (similar to batteries where the only difference is the transferred charge is proportional to voltage and its reversible). Moreover, pseudocapacitors exhibit higher energy density than the EDLCs because of the involvement of redox active material in storing charges both on the surface as well as in sub-surface layer [11]. Usually metal oxides are the suitable materials for pseudo-capacity. Generally, pseudocapacitance is associated with reversible Faradic redox processes

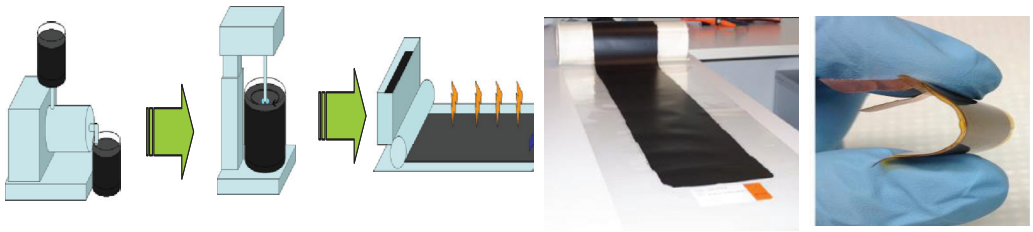

Figure 1. Left: schematics of the tape casting process including slurry formulation and tape cast. Center: image of the casted carbon nanofibers in a rolled tape. Right: flexibility of the CNF tape.

in various oxidation states of transition metal oxides (RuO_2, V_2O_5, MnO_2, NiO, and IrO_2). Among these oxide materials, MnO_2 has been recognized as a promising pseudocapacitive material since MnO_2 has a lower cost and is considered environment friendly than other metal transition oxides [3, 12]. However, the poor conductivity of MnO_2 (10^{-5}–10^{-6} S cm^{-1}) limits the charge/discharge rate for high power applications [13].

Recently, CNFs have gained much interest because of high surface area, mechanical stability, flexibility and relatively higher conductivity. Thus, the CNFs and metal oxide based nanocomposite can be engineered as a flexible supercapacitor. There are several studies on the fabrication of flexible supercapacitors based on the carbon material [10, 14–20]. Ma, *et al* assembled electrospun phenolic-based nanofibers and performed chemical treatment with KOH to obtained higher surface area [14]. In the study of Liu *et al* flexible porous carbon nanofibers exhibits a specific capacitance of 104 F g^{-1} at a current density of 0.2 A g^{-1} [15]. Zhi *et al* showed that addition of acetylacetonate in CNFs increase their surface area. The composite of acetylacetonate/CNFs/MnO_2 electrode delivers specific capacitance of 311 F g^{-1} at a scan rate of 2 mV s^{-1} [16]. Huang *et al* reported that multi material (CNFs/Co_3O_4/MnO_2) nanocomposite flexible electrode exhibits specific capacitance of 840 F g^{-1} at scan rate 5 mV s^{-1} based on the mass of MnO_2 [17]. D Zhou prepared hybrid nanostructured of MnO_2/Porous CNF electrode which presents high specific capacitance 520 F g^{-1} at 0.5 A g^{-1} [18]. Yang *et al* shown a simple method to introduce micropores without damaging a 3D mesoporous carbon nanonetwork structure [10]. Nataraj *et al* manufactured flexible thin film nanocomposited supercapacitor by *in situ* coprecipitation of 2D MnO_2 nanosheet in the presence of CNFs. They claimed a gravimetric capacitance of 142 F g^{-1} for CNFS-MnO_2 electrode interfaced with PVA-H4SiSiW12O40.nH_2O with slow scan rates [19]. Liu *et al* fabricated flexible supercapacitor sheets based on diverse materials such as carbon nanotubes, silicon, titanium oxide particles and graphene flakes, incorporated into the conducting polymer polyaniline to form nanocomposite which presents specific capacitance of 477.1 F g^{-1} [20].These reports suggest that flexible electrodes based supercapacitors are potential candidate for portable, wearable equipment. As far as we know there is no work in literature related to the use of low casting high dense carbon nanofiber alone and as in composite structure with MnO_2 for supercapacitors.

In the present work, a novel and flexible electrode based in carbon nanofibers has been developed. Various aqueous electrolyte concentrations were tested to obtain higher specific capacitance of flexible CNFs. The fast, easy and simple chemical treatment methods was used to treat CNFs with $KMnO_4$. Moreover, the effect of loading mass of MnO_2 deposited on the CNFs for supercapacitor were studied.

2. Experimental setup

Commercially available carbon nanofibers (CNFs), synthesized by CVD floating technique, developed by Grupo Antolín S.A., is used [21]. The diameters of the fibers are ranging from 30 to 80 nm and lengths up to several μm. For the preparation of electrodes, carbon nanofibers were casted by tape casting. This is a well-known process at industry in which powders are mixed with polymers and vehicle (organic or water) and later casted in a band for further processes [22, 23]. For the tape casting process, samples of carbon nanofibers where mixed with polymer in water as depicted in figure 1. In the first step the CNFs were gently dispersed in water in a pearls mill; in the second step, a slurry was formulated by mixing the water dispersed CNFs and a copolymer PE-PVAc (Celanese, Mowilith 1081 LDM) in a mechanical mixer under vacuum conditions. Different polymer concentration has been tested, a weight ratio 1:1 polymer to CNFs was considered for this work. Once the slurry was ready, the material was deposited using doctor blade system on a mylar© carrier and dried. The doctor blade carrier system and drying features were a CAM-H series Tape Casting Machine from KEKO equipment. The obtained tape is a homogeneous band without defects and pinholes of 500 mm wide and 75 μm thick. The optimized process produces 0.3 m h^{-1} [24]. Carrier was withdrawn prior to be used in supercapacitors.

The MnO_2/CNFs composite were synthesized via a direct redox reaction between $KMnO_4$ and CNFs based tape casting. The tape cast was cut into 10 mm diameter and immersed into a chemical treatment using $KMnO_4$ with different concentrations of 100, 450 and 1000 mg dissolved in 20 ml distilled water. The $KMnO_4$ solution was

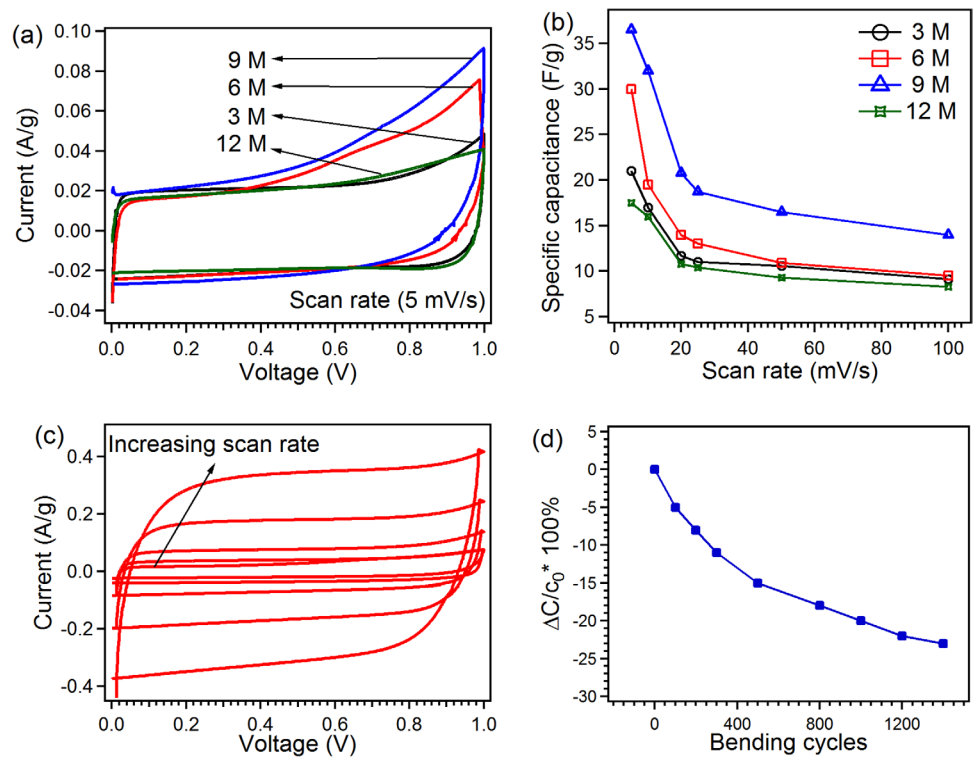

Figure 2. (a) Cyclic voltammogram comparison at a scan rate 5 mV s^{-1} for different concentration of KOH, (b) specific capacitance comparison at different scan rates, (c) cyclic voltammogram at different scan rates of (5, 10, 20, 25, 50 and 100 mV s^{-1}) for 6 M KOH as electrolyte, (d) capacitance retention as a function of bending numbers.

heated until the temperature reaches 47 °C. Afterwards, a 10 mm disc of CNFs was immersed in the solution for 10 min and was dried for 1 h at room temperature. The deposited loading masses of MnO_2 were 0.3, 0.41 and 0.6 mg for $KMnO_4$ concentrations 100, 450 and 1000 mg respectively. These loading masses were designated as S1, S2 and S3 respectively. The samples were tested using a two-electrode test cell. The electrochemical characterization (Cyclic Voltammetry, Galvanostatic charge discharge and Impedance spectroscopy) of CNFs alone and chemically treated with $KMnO_4$ CNFs, a disc was made in a Swagelok cell, using a Gamry 600 potentiostat. The glass microfiber filter (MFV5) was used as a separator. The surface morphology of CNFs and CNFs/MnO_2 composite electrode were studied by using scanning electron microscopy (SEM) (Jeol J-7100)and higher resolution transmission electron microscopy (HR-TEM) (JEOL JEM-2100, Japan). Raman spectroscopy measurement was performed to analyze the difference in the structure of CNFs and CNFs/MnO_2 using micro-Raman spectroscopy (HORIBA LabRam HR800, Japan. A green laser of wavelength 532 nm, 0.5 mW and a 50 LWD objective was used during the measurements. The specific surface area and pore size distribution of CNFs alone and in nanocomposite (CNFs/MnO_2) for samples S1, S2 and S3 were obtained by the N_2 adsorption/desorption isotherm using Micromeritics TriStar 3000 V6.04 A system.

3. Results and discussion

The electrochemical properties of CNFs as electrodes for supercapacitors were analyzed by using various concentrations of KOH (3, 6 9 and 12 M) as a suitable electrolyte for supercapacitors. In order to evaluate the supercapacitor performance, numerous methods were applied such as cyclic voltammetry, charge/discharge and impedance spectroscopy. First cyclic voltammetry was performed in the voltage window from 0 to 1 V. The specific capacitance per unit mass for one electrode was calculated using equation (1).

$$C_s = 4 * C/m \tag{1}$$

$$C = \frac{q_a + |q_c|}{\Delta V} \tag{2}$$

Where C_s is the specific capacitance in F g^{-1}, C is the measured capacitance for the two-electrode cell by equation (2) and m is the total mass of the active material in both electrodes [25]. In double layer capacitors it is important to achieve rectangular shaped cyclic voltammograms (CVs) for all scan rates. Figure 2(a) shows the comparison of different concentrations of KOH as electrolyte at a scan rate 5 mV s^{-1}. The mass of one electrode in each measurement

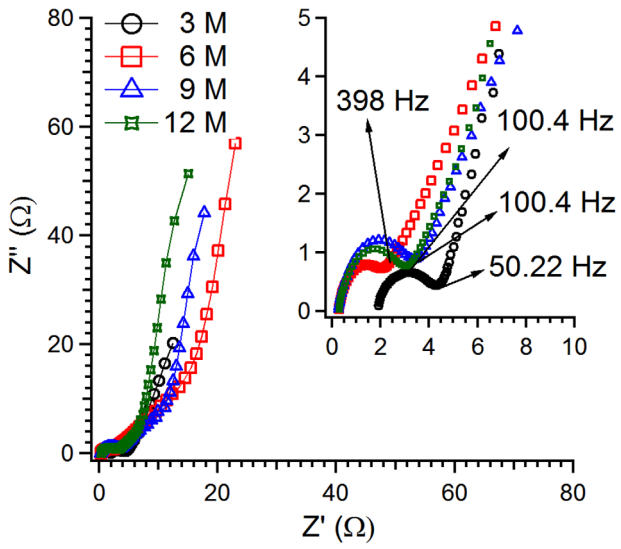

Figure 3. Nyquist plot at different electrolyte concentrations of KOH.

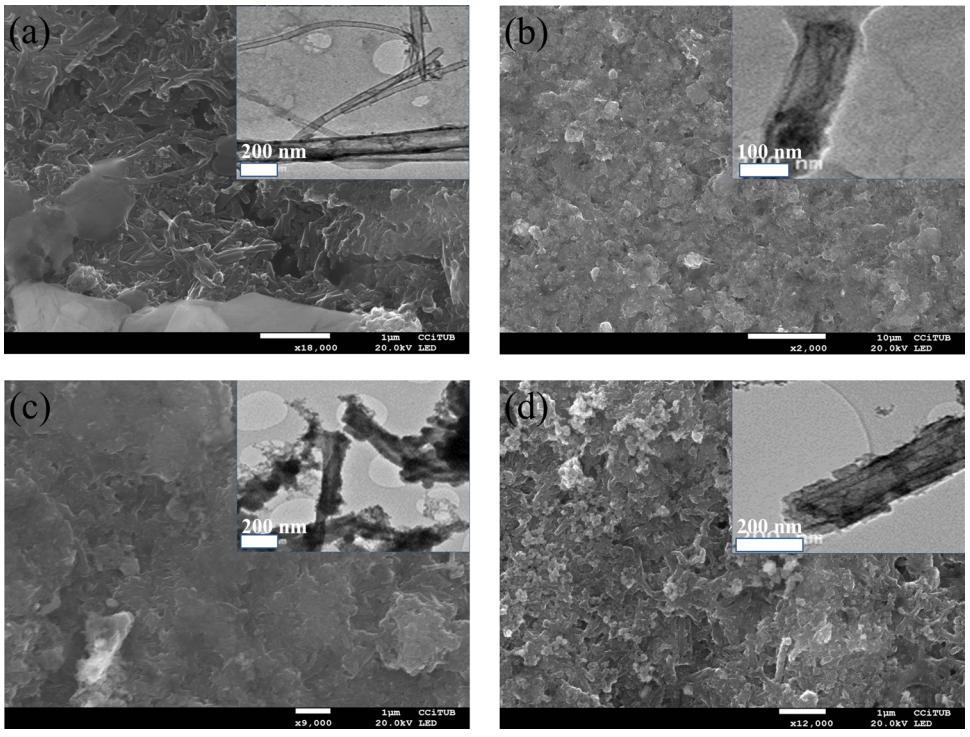

Figure 4. SEM images and TEM images (inset) for (a) CNFs, (b) S1, (c) S2 and (d) S3.

was ~0.0094 g. The rectangular shape CV is desirable for ideal double layer supercapacitor. However in our case the CV profiles for different concentrations presents irreversible cathodic hump at scan rate. This is possibly characteristic of Ni catalyst used in synthesis of CNFs and surface oxygen groups observed by EDX not shown here.

The integrated scan area for 9 M is higher than others. Figure 2(b) shows the specific capacitance comparison over a wide range of scans for all KOH concentrations. It can be seen that the calculated specific capacitance increases from 18 to 38 F g^{-1} for 3 M–9 M respectively, and decreases for 12 M at a scan rate 5 mV s^{-1}. It exhibits the higher electrolyte concentration provide higher ion concentration resulting in enhanced ion accessibilities onto the double layer surfaces [26]. But for much higher concentration of 12 M, capacitance is lower from all other electrolyte concentrations. These results interpret that very high electrolyte concentration 12 M may reduce the ion activity due to less water hydration, thus resulting in decrease in mobility [27]. Another reason could be that the KOH only can be dissolved in the water up to a certain limit. In supersaturation state excess amount of KOH will remain in the state of solid as undissolved salt crystal in the solution. This solid-state crystals disturb the conductive path of the solution hence decrease the conductive pathways of the electrolyte.

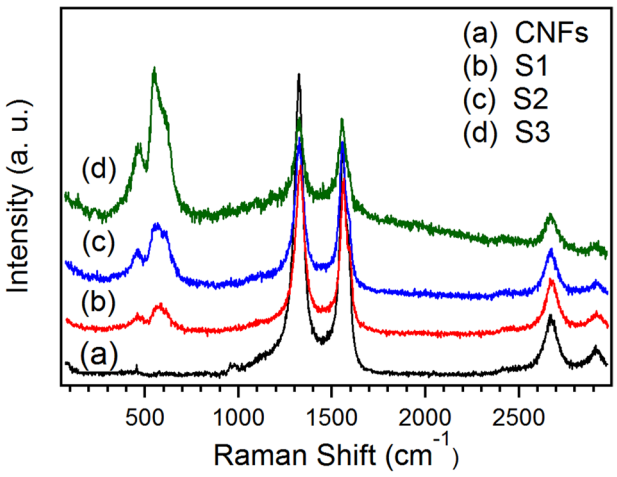

Figure 5. Raman spectra of CNFs, S1, S2 and S3.

Figure 2(c) shows the CVs at different scan rates for 6 M concentration. At the entire scan rates CV curves exhibit almost rectangular shapes, fast current response to the change of voltage sweep directions indicates the highly capacitive nature with good ion response. Therefore, we can say that the contribution of pseudo capacitance to total capacitance of the supercapacitor is negligible; the overall specific capacitance is mainly associated to double layer capacitance. The supercapacitor is flexible and stretchable. It can be bent in any direction without degradation in performance. The specific capacitance remained at 74% after 1200 bending cycle shown in figure 2(d).

The electrochemical characteristics of the electrode and electrolyte were further realized by impedance spectroscopy. The impedance measurements were carried out at AC with 10 mV amplitude over a frequency range between 100 kHz and 0.1 Hz. Figure 3 shows the Nyquist plot of the CNFs with different electrolyte solution concentrations.

The equivalent circuit of a supercapacitor based on porous electrodes and electrolyte presents a complex combination of capacitance (C) and resistance (R) components. The interfacial impedance of a supercapacitor is associated with a double-layer capacitance C_{dl}, pseudocapacitance C_p, Faradaic charge-transfer resistance R_f, the sum of the electrolyte resistance, the electrode resistance, the contact resistance between the electrode and the current collector R_s [28, 29].

The Nyquist plots consist of a high-frequency intercept on the real Z_{Re} axis, a semicircle in the high-to-medium-frequency region, and a straight line at the very low-frequency region. The solution resistance R_s for 3 M was about 1.9 Ω higher than other concentrations which are about 0.1 Ω for all others. The semicircle from high to medium frequency which corresponds to Faradaic charge transfer resistance (R_f) of electrode material was 4.3, 2, 3 and 2.9 Ω for 3, 6, 9 and 12 M KOH concentrations respectively. This indicates that the moderated concentrated solution increases the ionic conductivity in the porous structure of the electrode. It can be seen that a semicircle in the high frequency region and almost a straight line parallel to Z_{img} axis, tells that the supercapacitors have a resistive behavior at high frequencies and a capacitive behavior at low frequencies. The knee frequency represents the maximum frequency where the capacitive behavior is dominant as well as power capability of the supercapacitor. The highest knee frequency 398 Hz was obtained for 6 M, which explains exactly polarized system as shown in figure 3. These electrochemical characterization demonstrate that relatively higher capacitance with lower ESR can be obtained with 6 M KOH. The optimized KOH electrolyte concentration with lower charge transfer resistance, small ESR and moderate specific capacitance was 6 M. Therefore, further experiments for nanocomposites of manganese and CNFs, 6 M KOH electrolyte solution were chosen.

The surface morphology of CNFs and CNFs/MnO_2 composite electrode were studied by using SEM and TEM figure 4. Figure 4(a) shows the structure of the entangled CNFs as received. Figure 4(b) corresponds to S1 sample, where MnO_2 is homogeneously distributed as a thin layer uniformly covering the surface of CNFs. It is very important to achieve a conformal coating of MnO_2 on the surface of CNFs without losing the electronic and ionic conductivity through the electrode. Figure 4(c) S2 sample shows that deposited MnO_2 layer on CNFs is thicker than for S1. Figure 4(d) S3 shows that MnO_2 is randomly deposited as a thick film and as well as nanosphere-like structures at different places.TEM images show significantly altered CNFs structure after the treatment with KMnO4 figure 4 (insets). MnO_2nanoclusters (thin film) around CNFs for S1 are barely visible because of small thickness. However, with increase in loading mass for S2 and S3 the thickness of MnO_2 is increased.

Raman spectroscopy measurement was performed to analyze the difference in the structure of CNFs and CNFs/MnO_2 composite. Figure 5 shows very well pronounced distinct peaks for MnO_2/CNFs sample at 490, 560, and 640 cm^{-1} are whose positions are similar to those described in the literature for MnO_2 Raman spectra [12, 30,

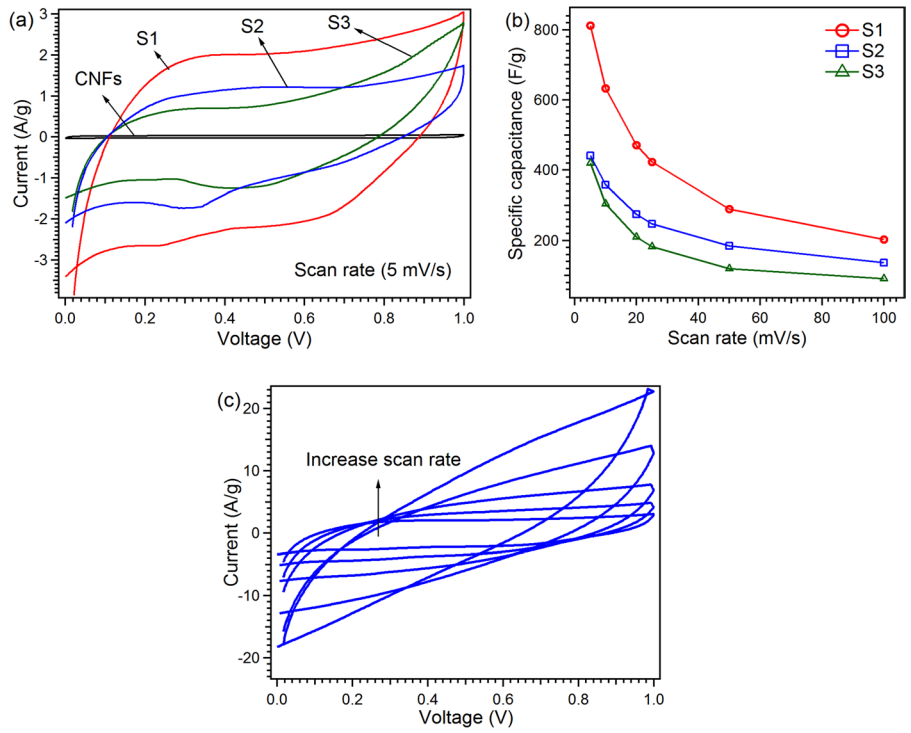

Figure 6. (a) Cyclic voltammetry comparison between various samples at 5 mV s^{-1} scan rate, (b) specific capacitance comparison at different scan rates, (c) cyclic voltammograms at different scan for S1 (5, 10, 20, 25, 50 and 100 mV s^{-1}).

31]. The locations (~1365 cm^{-1}) and (~1580 cm^{-1}) are attributed to the D and G bands of carbon, corresponding to the defect and disorder induced structures and the vibrations of carbon atoms with sp^2 electronic configuration in CNFs respectively [32].

Figure 6(a) shows the cyclic voltammograms comparison at a scan rate of 5 mV s^{-1} between CNFs and nanocomposite of CNFs/MnO_2. CVs of nanocomposites (S1, S2 and S3) are little deviated from the rectangular shape with humps at different potentials from 0.2 to 0.7 V. The CV deviation is related to the slow diffusion of ions on the surface and into the bulk of the material. The peaks are due to reversible Faradaic reactions in various oxidation states of manganese. The appearance of these peaks describes that the charge storage mechanism is transferred from double layer to pesudocapacitance because of redox reactions of MnO_2 [19]. The specific capacitance was calculated by using the equation (1) and considering the deposited mass of MnO_2 as an active material [3, 12].The electrochemical kinetics of an electrode defines the power characteristics of an electrode material. It was observed that S1 provides the larger specific current and specific capacitance. Figure 6(b) exhibits the specific capacitance of CNFs/MnO_2 at different scan rates, which shows that as the scan rates increase, the specific capacitance decreases. This decrease is possibly due to the limited ions transfer to the interior pores of the electrode materials at high scan rates [27].

The sample S1 shows highest specific capacitance about 812 F g^{-1} higher than the corresponding values for S2 and S3 and retains its specific capacitance at larger value 203 F g^{-1} even at higher scan rate 100 mV s^{-1}. Retention of specific capacitance even at fast scan rate is desirable characteristics for high power supercapacitors. The higher specific capacitance of CNF/MnO_2 is due to combination of two charge storage mechanism, those are double layer capacitance and reversible redox reactions at the surface and in bulk of the active material [33]. The thickness of MnO_2 for S2 and S3 is higher, therefore the SC decreases as the film thickness increases due to the low conductivity of MnO_2 [34]. Figure 6(c) shows that with increase in scan rate the shape of CV deviates from rectangular shape due to the internal resistance of the electrode, which obstructs the diffusion of the ions.

Galvanostatic charge/discharge curves were measured applying various current densities from 4 to 16 A g^{-1}. Figure 7(a) shows the charge/discharge curves for S1 sample at different currents densities. The discharge capacitance (C) was estimated from the slope (dV/dt) of the linear portion of the discharge curve using equation (3).

$$C_s = \left(\frac{2I}{(dV/dt) \cdot m} \right) \tag{3}$$

Where C_s is the specific capacitance in F g^{-1}, I is the discharge current in A, dV is the voltage difference during the discharge curve in V, dt the discharge time in sand m is the mass of active material (MnO_2). As charge discharge current increases, the voltage drop (IR) goes larger, and the capacitance decreases. The calculated highest specific

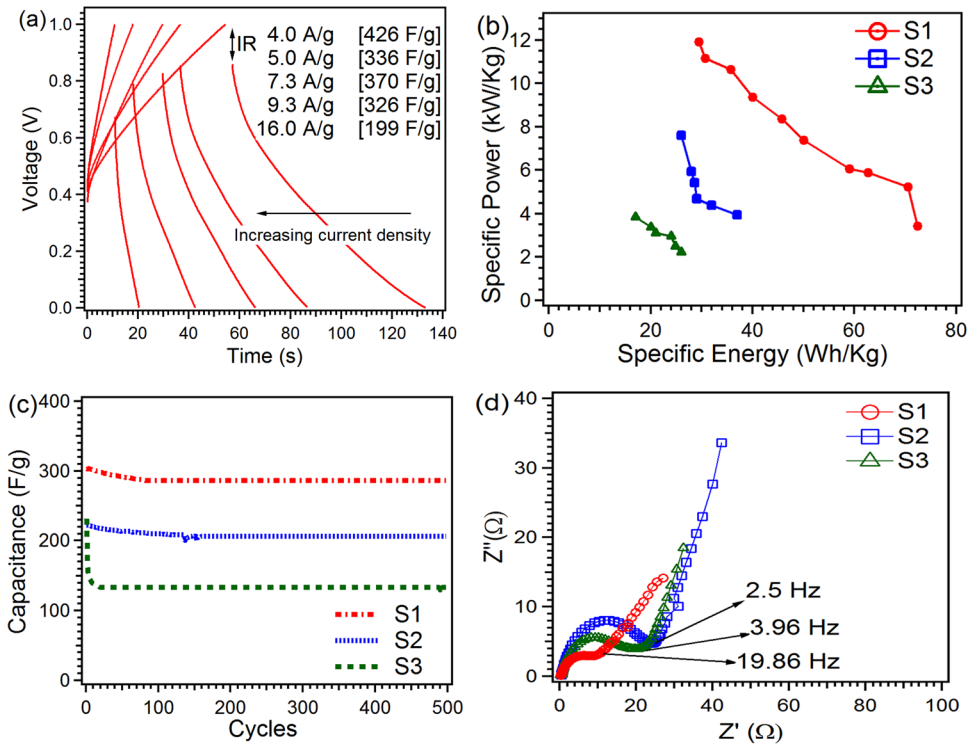

Figure 7. (a) Charge /discharge curves at different current for S1, (b) ragone plot of specific power against specific energy for S1, S2 and S3, (c) charge/discharge cyclic stability of supercapacitors with S1, S2 and S3, (d) Nyquist plot for S1, S2 and S3.

capacitance 426 F g^{-1} obtained at 4 A g^{-1} decrease to 199 F g^{-1} at current 16 A g^{-1}. It shows that nanocomposite retain the higher capacitance even at higher currents.

Specific energy and specific power are important parameters to analyse the electrochemical performance of energy storage devices. The specific power, P and specific energy, E, delivered upon discharge were estimated by equation (4) and (5) [35].

$$P = {Vi}/{m} \tag{4}$$

$$E = {Vit}/{m} \tag{5}$$

Where V is the voltage excluding IR drop, i is discharge current, and t is the discharge time in s and m is the mass of active material (MnO_2).

Figure 7(b) shows the Ragone plot for the S1, S2 and S3 at different current densities. The S1 shows highest energy 72.4 Wh kg^{-1} at 3.44 kW kg^{-1} at current density of (4 A g^{-1}) and decrease slowly to 29.5 Wh kg^{-1} at relatively very high power 11.91 KW kg^{-1} at a current density (18 A g^{-1}). The specific power and energy for S2 and S3 are much lower than S1.

Cycling stability of the nanocomposite was investigated applying up to 500 galvanostatic charge/discharge cycles at different current densities 7.9, 5.7, and 3.8 A g^{-1} for S1, S2 and S3 respectively in the range of 0–1 V Figure 7(c). The discharge capacitance (C) is estimated from the slope (dV/dt) of the linear portion of the discharge curve using the equation (3). It is evident that S1 exhibits higher capacitance 303 F g^{-1} and capacitance retention in comparison with S2 and S3. For S3 the capacitance fading from 231 to 138 F g^{-1} in the first 10 cycles was observed, which is due to the thicker and random structure of MnO_2 on the CNFs.

Electrochemical impedance spectroscopy was performed to investigate the kinetics behavior of hybrid electrodes. The solution resistance for all samples was almost similar ~0.3 Ω, whereas the Faradaic charge transfer resistance R_f varies. The R_f was ~9, 23 and 20 Ω for S1, S2 and S3 respectively see figure 7(d). The R_f of S2 and S3 is higher possibly because of thicker and random structure of MnO_2. The Nyquist plot of the samples present an almost straight line parallel to the imaginary axis that describes exactly polarized systems. Deviation from this vertical line at low frequencies to smaller slopes corresponds to a higher contribution of the ionic diffusion resistance. The knee frequency of S1 was 19.86 Hz higher that of S2 and S3.

To understand the influence of surface area and pore size distribution of CNFs, S1, S2 and S3 samples on the specific capacitance BET analysis were performed. The textural properties of all samples were evaluated by collecting the nitrogen sorption isotherms, as shown in figure 8(a). The isotherms present a small hysteresis loop from higher to middle pressure range, which is the indication of meso and macro porous structure. According to

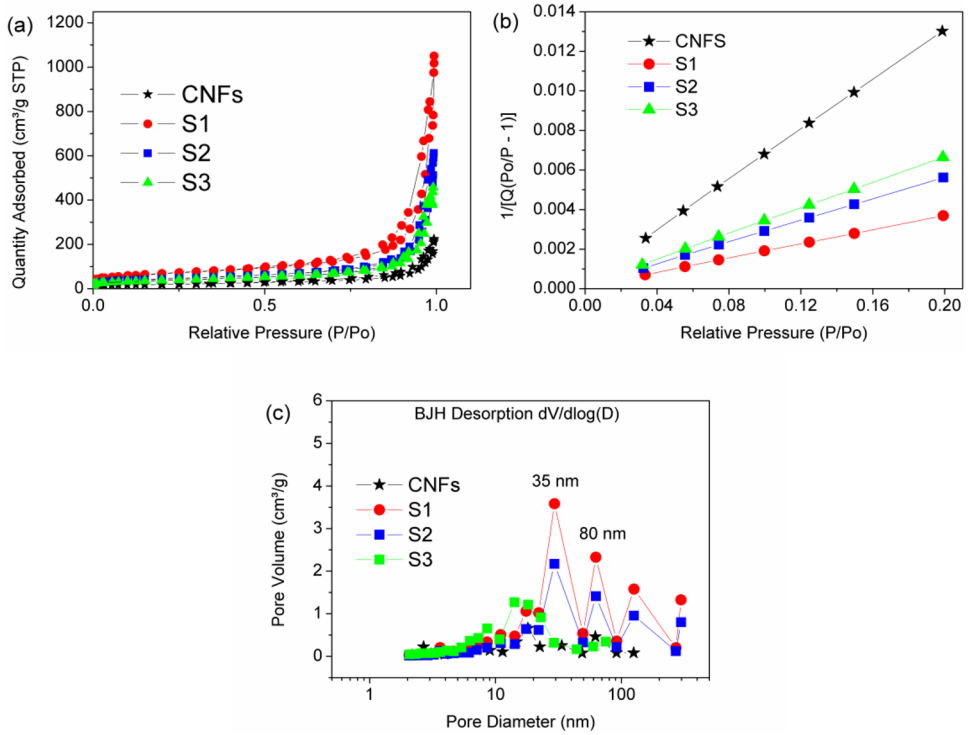

Figure 8. (a) Nitrogen adsorption/desorption isotherms, (b) BET surface area, (c) pore size distribution.

Table 1. Pore parameters for CNFs and CNFs/MnO_2.

Sample	S_{BET} ($m^2\ g^{-1}$)	S_{micro} ($m^2\ g^{-1}$)	S_{mesoo} ($m^2\ g^{-1}$)	S_{macra} ($m^2\ g^{-1}$)	V_{total} ($cm^3\ g^{-1}$)	V_{micro} ($cm^3\ g^{-1}$)	V_{meso} ($cm^3\ g^{-1}$)	V_{macra} ($cm^3\ g^{-1}$)
CNFs	68	4.8	50.2	13	0.34	0.001	0.188	0.152
S1	240	59	153	28	1.63	0.13	0.85	0.65
S2	148	36	93	19	0.98	0.03	0.439	0.511
S3	133	27	87.5	18.5	0.7	0.001	0.38	0.32

S_{BET} = BET surface area, S_{micro} = micropore surface area, S_{meso} = mesopore surface area, S_{macra} = macrapore surface area, V_{total} = total volume, V_{micro} = micropore volume, V_{meso} = mesopore volume, V_{macra} = macrapore volume.

IUPAC classification the isotherm of sample can be classified as type II and type IV isotherm [36]. The total volume of pores (V_{total}, $cm^3\ g^{-1}$) was calculated by the number of adsorbed nitrogen at P/P0 ≈ 0.9932. The volume of micropores and the values of surface areas of micro (S_{micro}, $m^2\ g^{-1}$) were investigated by the use of t-Plot Harkins and Jura method. The total pore volume for S1 (1.63 $cm^3\ g^{-1}$) is about 4.8 times higher than CNFs, about 1.66 times higher than S2 and about 2.32 times higher than S3. The pore volume distribution is presented in table 1. The surface area (BET) was determined by multiple point Brunauer–Emmett–Teller (BET) method in the region of the isotherm, which is limited by the range of relative pressure $P/P_0 = 0.02$–0.2 as seen in figure 8(b). The adsorption volume shows that BET surface areas for CNFs, S1, S2 and S3 are 68, 240, 148 and 133 $m^2\ g^{-1}$ respectively.

The pore size distribution of the materials is classified into three groups: micro pores (<2 nm), meso pores (2–50 nm) and macro pores (>50 nm) [37]. The pore size distributions were calculated from adsorption isotherms by the Barrett−Joyner−Halenda (BJH) method. Figure 8(c) presents the pores of all sample are mainly distributed in between meso and macro pores. The dominant pores sizes for S1 and S2 are centered in the range of 20, 35 and 80 nm. While the main pore size distribution for S3 is (8 and 20 nm) and for CNFs (2.5, 20 and 80 nm) figure 8(c). The correlation between BET results and specific capacitance can be understand by equation $C = \varepsilon A/d$ where ϵ is electrolyte dielectric constant, A is the surface area accessible to ions and d is the distance from ions to the pore surface of electrode on the order of angstrom. According to the above equation, two approaches can be taken to enhance the charge storage of supercapacitors effectively: increasing the specific surface area and reducing the distance between ions and the surface of the electrode. The BET results reveal that S1 have higher specific surface area and higher number of mesopores. The high surface area and large amount of mesopore structures provide the possibility of efficient transport of electrons and ions, which leads to the high electrochemical capacitance. Beside this the thickness of MnO_2 film plays an important role during charging and discharging supercapacitor. It is evident that the thickness of the electrode S1 is much thinner than that of the S2, S3 and CNFs figure 4. Hence, it can be

speculated that a longer distance of ionic motion in the electrodes of S2, S3 and CNFs is necessary from electrolyte to the inner MnO_2. The thinner film sample S1 delivers higher specific capacitance in comparison to S2 and S3.

4. Conclusions

The supercapacitor performance of flexible Carbon nanofibers (CNFs) electrodes in different concentrations of KOH was investigated. It was found that the specific capacitance increased to 38 F g^{-1} with increasing concentration up to 9 M, beyond this value specific capacitance decreased due to undissolved salt and ion mobility. A fast and easy method to obtain a hybrid nanostructure having uniform distribution of MnO_2 on the CNFs has been introduced. The chemical treatment of CNFs with different concentration of $KMnO_4$ solution at moderate temperature for 10 min has been performed obtaining different structures of MnO_2. SEM images shows that the less concentrated (0.1 g $KMnO_4$) favor the even thinner coating of MnO_2 on the surface of CNFs. Raman results tells us that the manganese is in MnO_2 oxidation state. The highest specific capacitance is 812 F g^{-1}, low Faradaic charge transfer resistance (~9 Ω), long cycling stability with higher capacitance (303 F g^{-1}) at current of 7.9 A g^{-1} was achieved when MnO_2 is uniformly in contact as a thin film with the surface of CNFs and containing high BET surface area. Moreover, the highest energy density of 72.4 Wh kg^{-1} at 3.44 kW kg^{-1} specific power was calculated.

Acknowledgments

A Daraghmeh acknowledges the European Union grant for PhD grant in Erasmus Mundus AVEMPACE III program. A. Cirera acknowledges support from the 2015 edition of BBVA Foundation Grants for Researchers and Cultural Creators. The ACCIÓ project RD14-1-0068 of the Generalitat de Catalunya under FEDER founds of the European Union founded this work.

References

[1] Claramunt S, Monereo O, Boix M, Leghrib R, Prades J D, Cornet A, Merino P, Meriono C and Cirera A 2013 Flexible gas sensor array with an embedded heater based on metal decorated carbon nanofibers *Sensors Actuators* B **187** 401–6
[2] Huang Y, Candelaria S L, Li Y, Li Z, Tian J, Zhang L and Cao G 2014 Sulfurized activated carbon for high energy density supercapacitors *J. Power Sources* **252** 90–7
[3] Amade R, Jover E, Caglar B, Mutlu T and Bertran E 1965 Optimization of MnO_2/vertically aligned carbon nanotube composite for supercapacitor application *J. Power Sources* **1965** 779–5783
[4] Hussain S, Amade R, Jover E and Bertran E 2013 Nitrogen plasma functionalization of carbon nanotubes for supercapacitor applications *J. Mater. Sci.* **18** 7620–8
[5] Hussain S, Amade R, Jover E and Bertran E 2012 Functionalization of carbon nanotubes by water plasma *Nanotechnology* **23** 385604
[6] Jung K H, Denga W, Smith D W Jr and Ferraris J P 2012 Carbon nanofiber electrodes for supercapacitors derived from new precursor polymer: poly (acrylonitrile-co-vinylimidazole) *Electrochem. Commun.* **23** 149–52
[7] Wu Z S, Parvez K, Feng X and Mullen K 2013 Graphene-based in-plane micro-supercapacitors with high power and energy densities *Nat. Commun.* **4** 2487
[8] Yang X, Zhang G, Zhong M, Wu D and Fu R 2014 Ammonia-assisted semicarbonization: a simple method tointroduce micropores without damaging a 3D mesoporous carbon nanonetwork structure *Langmuir* **30** 9183–9
[9] Li C, Yang X and Zhang G 2015 Mesopore-dominant activated carbon aerogels with high surface area for electric double-layer capacitor application *Mater. Lett.* **161** 538–41
[10] Yang X, Li C and Fu R 2016 Nitrogen-enriched carbon with extremely high mesoporosity and tunable mesopore size for high-performance supercapacitors *J. Power Sources* **319** 66–72
[11] Yang D 2012 *Application of Nanocomposites for Supercapacitors: Characteristics and Properties* (Rijeka: Intech) ch 12
[12] Hussain S, Amade R, Jover E and Bertran E 2013 Water plasma functionalized CNTs/MnO_2 composites for supercapacitors *Sci. World J.* **2013** 832581
[13] Lang X, Hirata A, Fujita T and Chen M 2011 Nanoporous metal/oxide hybrid electrodes for electrochemical supercapacitors *Nat. Nanotechnol.* **6** 232–6
[14] Ma C, Li Y, Shi J, Song Y and Liu L 2014 High-performance supercapacitor electrodes based on porous flexible carbon nanofiber paper treated by surface chemical etching *Chem. Eng. J.* **249** 216–25
[15] Liu Y, Zhou J, Chen L, Zhang P, Fu W, Zhao H, Ma Y, Pan X, Zhang Z, Han W and Xie E 2015 Highly flexible freestanding porous carbon nanofibers for electrodes materials of high-performance all-carbon supercapacitors *ACS Appl. Mater. Interfaces* **7** 23515–20
[16] Zhi M, Manivannan A, Meng F and Wu N 2012 Highly conductive electrospun carbon nanofiber/MnO_2 coaxial nano-cables for high energy and power density supercapacitors *J. Power Sources* **208** 345–53
[17] Huang Y, Miao Y E, Tjiu W W and Liu T 2015 High-performance flexible supercapacitors based on mesoporous carbon nanofibers/Co_3O_4/MnO_2 hybrid electrodes *RSC Adv.* **5** 18952–9
[18] Zhou D, Lin H, Zhang F, Niu H, Cui L, Wang Q and Qu F 2015 Freestanding MnO_2nanoflakes/porous carbon nanofibers for high-performance flexible supercapacitor electrodes *Electrochim. Acta* **161** 427–35
[19] Nataraj S K, Song Q, Al-Muhtaseb S A, Dutton S E, Zhang Q and Sivaniah E 2013 Thin flexible supercapacitors made from carbon nanofiber electrodes decorated at room temperature with manganese oxide nanosheets *J. Nanomater.* **2013** 6
[20] Liu Q, Nayfeh O, Nayfeh M H and Yau S T 2013 Flexible supercapacitor sheets based on hybrid nano composite materials *Nano Energy* **2** 133–7
[21] Vera-Agullo J, Varela-Rizo H, Conesa J A, Almansa C, Merino C and Martin-Gullon I 2007 Evidence for growth mechanism and helix-spiral cone structure of stacked-cup carbon nanofibers *Carbon* **45** 2751–8

[22] Hu X B, Zhao B Y and Hu K A 2004 A novel fabrication of doped C/C composite laminations by aqueous tape casting *Acta Mater.* **52** 467–73
[23] Korkut S, Roy-Mayhew J D, Dabbs D M, Milius D L and Aksay I A 2011 High surface area tapes produced with functionalized graphene *ACS Nano* **5** 5214–22
[24] Ramos F M 2014 Integración de la tecnología cerámica multicapa *PhD Thesis* University of Barcelona
[25] Stoller M D and Ruoff R S 2010 Best practice methods for determining an electrode material's performance for ultracapacitors *Energy Environ. Sci.* **3** 1294–301
[26] Azam M A, Fujiwara A and Shimoda T 2013 Significant capacitance performance of vertically aligned single-walled carbon nanotube supercapacitor by varying potassium hydroxide concentration *Int. J. Electrochem. Sci.* **8** 3902–11
[27] Tsay K-C, Zhang L and Zhang J 2012 Effects of electrode layer composition/thickness and electrolyte concentration on both specific capacitance and energy density of supercapacitor *Electrochim. Acta* **60** 428–36
[28] Liu C G, Liu M, Li F and Cheng H M 2008 Frequency response characteristic of single-walled carbon nanotubes as supercapacitor electrode material *Appl. Phys. Lett.* **92** 143108
[29] Hussain S, Amade R and Bertran E 2014 Study of CNTs structural evolution during water assisted growth and transfer methodology for electrochemical applications *Mater. Chem. Phys.* **148** 914–22
[30] Buciuman F, Patcas F, Craciun R and Zahn D R T 1999 Vibrational spectroscopy of bulk and supported manganese oxides *Phys. Chem. Chem. Phys.* **1** 185–90
[31] Bernard M-C, Goff A H-L, Thi B V and De Torresi S C 1993 Electrochromic reactions in manganese oxides *J. Electrochem. Soc.* **140** 3065–70
[32] Yue H, Li F, Yang Z, Li X, Lin S and He D 2014 Facile preparation of Mn_3O_4-coated carbon nanofibers on copper foam as a high-capacity and long-life anode for lithium-ion batteries *J. Mater. Chem.* A **2** 17352–8
[33] Tran V M, Ha A T and Le M L P 2014 Capacitance behavior of nanostructured ε-MnO_2/C composite electrode using different carbons matrix *Adv. Nat. Sci. Nanosci. Nanotechnol.* **5** 025005
[34] Nagarajan N, Cheong M and Zhitomirsky I 2007 Electrochemical capacitance of MnO_x films *Mater. Chem. Phys.* **103** 47–53
[35] Farma R, Deraman M, Awitdrus A, Talib I A, Omar R, Manjunatha J G, Ishak M M, Basri N H and Dolah B N M 2013 Physical and electrochemical properties of supercapacitor electrodes derived from carbon nanotube and biomass carbon *Int. J. Electrochem. Sci.* **8** 257–73
[36] Gregg S J and Sing K S W 1982 *Adsorption, Surface Area and Porosity* 2nd edn (New York: Academic) pp 4, 287
[37] Huang J, Sumpter B G and Meunier V 2008 A universal model for nanoporous carbon supercapacitors applicable to diverse pore regimes *Chemistry* **14** 6614–26